$N^* \to N\eta'$ decays from photoproduction of η'-mesons off protons

A. V. Anisovich[a,b], V. Burkert[c], P. M. Collins[d], M. Dugger[d], E. Klempt[a,c], V. A. Nikonov[a,b], B. G. Ritchie[d], A. Sarantsev[a,b], U. Thoma[a]

[a]*Helmholtz–Institut für Strahlen– und Kernphysik, Universität Bonn, Germany*
[b]*NRC "Kurchatov Institute", PNPI, Gatchina 188300, Russia*
[c]*Thomas Jefferson National Accelerator Facility, Newport News, Virginia 23606*
[d]*Arizona State University, Tempe, Arizona 85287-1504*

Abstract

A study of the partial-wave content of the $\gamma p \to \eta' p$ reaction in the fourth resonance region is presented, which has been prompted by new measurements of polarization observables for that process. Using the Bonn-Gatchina partial-wave formalism, the incorporation of new data indicates that the $N(1895)1/2^-$, $N(1900)3/2^+$, $N(2100)1/2^+$, and $N(2120)3/2^-$ are the most significant contributors to the photoproduction process. New results for the branching ratios of the decays of these more prominent resonances to $N\eta'$ final states are provided; such branches have not been indicated in the most recent edition of the Review of Particle Properties. Based on the analysis performed here, predictions for the helicity asymmetry E for the $\gamma p \to \eta' p$ reaction are presented.

Keywords: baryon spectroscopy, meson photoproduction, polarization observables

1. Introduction

The cross section for pion-nucleon elastic scattering as a function of center-of-mass energy W reveals four distinct but broad energy ranges where enhancements are observed, which are called resonance regions. The first resonance region is principally due to $\Delta(1232)3/2^+$ formation, which dominates the cross section at low masses. Somewhat higher in W, the second resonance region houses the $N(1520)3/2^-$ as the leading resonance, along with contributions from the $N(1440)1/2^+$ and $N(1535)1/2^-$ excitations. At still higher W, several well-known resonances contribute to the third resonance region, in particular the $N(1680)5/2^+$ state. At $1900 \le W \le 2100$ MeV, the fourth resonance region appears as a small peak-like structure in the total πN cross section, which is largely due to the $\Delta(1950)\ 7/2^+$ excitation with substantial contributions from other Δ^* resonances.

Interestingly, N^* resonance contributions to the fourth resonance region have been difficult to identify, and these contributions are presently under study in a number of experiments. Photoproduction of η'-mesons offers the chance to search for low-spin high-mass nucleon resonances in the region above $W = 1900$ MeV. Due to isospin conservation, the reaction $\gamma p \to \eta' p$ receives contributions only from N^* intermediate states, and thus the reaction functions as an "isospin filter" for the nucleon resonance spectrum, helping isolate those N^* states. Furthermore, due to the angular momentum barrier, high-spin resonances are suppressed. Consequently, the photoproduction of η' mesons can be expected to shed light on the low-spin N^* resonances in the fourth resonance region.

Photoproduction of η'-mesons was first studied at DESY in a hydrogen bubble chamber [1] and a streamer chamber [2], though only a few events were observed for incident photon energies up to 6.3 GeV. At ELSA in Bonn, the reaction was investigated with the magnetic spectrometer SAPHIR in the energy range from 900 to 2600 MeV; 250 events due to η' production were reported. The linear forward rise of the angular distribution was assigned to two resonances with $J^P = 1/2^\pm$ [3]. Within the MAID model, the SAPHIR data were described by the interference of a $J^P = 1/2^-$ resonance and the exchange of a t-channel Regge trajectory [4]. When the new data from CLAS on η' photoproduction on the proton for 1935 MeV $< W <$ 2249 MeV [5] were included in the fit, four resonances with $J^P = 1/2^\pm$ and $J^P = 3/2^\pm$ were required to achieve a good description [6] of the data. Huang, Haberzettl, and Nakayama [7] included additionally data on the differential cross sections on η' photoproduction off protons from the CLAS collaboration, which covered the range from the production threshold up to $W = 2840$ MeV [8], and the CBELSA/TAPS data off protons [9] and off nucleons bound in the deuteron [10] taken from the production threshold up to $W = 2380$ MeV. The fit required a subthreshold contribution of $N(1720)3/2^+$ and three above-threshold resonances with quantum numbers $J^P = 1/2^\pm$ and $3/2^+$. Recently, the A2 Collaboration at MAMI studied the reaction $\gamma p \to \eta p$ and $\to \eta' p$ [11]. A strong cusp is observed in the η excitation functions in vicinity of the η' threshold. Within the η-MAID isobar model, the cusp is interpreted by production of the $N(1895)1/2^-$ nucleon resonance and its significant decay branching ratios to both,

to $N\eta$ and $N\eta'$. Indeed, all analyses agree that the threshold in η' photoproduction is governed by a resonance with $J^P = 1/2^-$ and a mass of about $1900\,\text{MeV}$. In addition, there is evidence for $N(2100)1/2^+$, and contributions from a $3/2^+$ resonance from a $3/2^-$ resonance also have been suggested.

Partial-wave analyses benefit tremendously from data on meson photoproduction observables obtained when different relative orientations of the spin of the incident photon or the struck nucleon (or both) are available (so-called "polarization observables"). Such data are now becoming available for the $\gamma p \to \eta' p$ reaction. Recently, the GRAAL collaboration reported a measurement of the linearly-polarized photon beam asymmetry Σ for η' photoproduction on unpolarized protons near threshold [12]. More recently, the CLAS collaboration [13] also measured Σ over an extended mass range from threshold up to $2092\,\text{MeV}$. These new data on Σ stimulated us to study the partial-wave content of the $\gamma p \to \eta' p$ reaction using a model that also describes simultaneously data for the photoproduction of other mesons as well. Such multi-channel analyses can provide great insight into the nucleon resonance spectrum since the strengths of the decay modes for the various resonances participating in the process vary greatly from one final state to another.

2. Formalism

For the investigation reported here, a partial-wave analysis was performed with the Bonn-Gatchina (BnGa) formalism, described more fully elsewhere [14, 16–18]. Briefly, this approach uses a modified K-matrix in the form

$$\hat{\mathbf{A}}(s) = \hat{\mathbf{K}}\,(\hat{\mathbf{I}} - \hat{\mathbf{B}}\hat{\mathbf{K}})^{-1} \qquad (1)$$

that is defined in the complex s plane. On the real axis, $\sqrt{s} = W$. The K-matrix elements combine the contributions from resonances and from background through

$$K_{ab} = \sum_\alpha \frac{g_a^\alpha g_b^\alpha}{M_\alpha^2 - s} + f_{ab}\,. \qquad (2)$$

Here, $g_{a,b}^\alpha$ are coupling constants of the pole α to the initial state a and the final state b. M_α defines the K-matrix pole (which differs from the T-matrix pole which is listed in the RPP). f_{ab} represents non-resonant background contributions. f_{ab} could be functions of s but in practice, a constant term is sufficient to achieve good fits. Only for the $J^P = 1/2^-$ wave, a more complicated expression was used:

$$f_{ab}(s) = \frac{f_{ab}^{(1)} + f_{ab}^{(2)}\sqrt{s}}{s - s_0^{ab}} \qquad (3)$$

where $f_{ab}^{(1)}$, $f_{ab}^{(2)}$, s_0^{ab} are constants determined in the fit.

The multi-channel amplitude $\hat{\mathbf{A}}(s)$ with matrix elements $A_{ab}(s)$ defines the transition amplitude from channel a to channel b. $\hat{\mathbf{B}}$ is a diagonal matrix with an imaginary part given by the corresponding phase space volume

$$\hat{B}_i = \Re e B_i + i\rho_i\,, \qquad (4)$$

where $\Re e B_i$ is calculated from the dispersion integral with one subtraction regularization. In addition to this modified K-matrix, we have also included a Regge-ized amplitude describing the exchange of vector mesons in the t-channel [18]. For the fits of the existing data with this approach, we restricted the mass range to $W \leq 2360\,\text{MeV}$ since many nucleon resonances will contribute to the process at high incident photon energies, making it difficult to identify the leading contributions.

In the reaction $\gamma p \to \eta' p$, the coupling constants in the initial and the final state are weak. In this case, a simplified amplitude can be used

$$A_f^h = \hat{G}_f + \hat{P}_a[(\hat{I} - \hat{B}\hat{K})^{-1}\,\hat{B}]_{ab}\hat{D}_{bf}\,. \qquad (5)$$

The transition from the initial γN state to the K-matrix channel a is represented by

$$\hat{P}_a = \sum_\alpha \frac{g_{\gamma N}^{(\alpha)} g_a^\alpha}{M_\alpha^2 - s} + F_a \qquad (6)$$

where $g_{\gamma N}^{(\alpha)}$ are resonance couplings and F_a describes the non-resonant transition.

$$\hat{D}_{bf} = \sum_\alpha \frac{g_b^{(\alpha)} g_f^{(\alpha)}}{M_\alpha^2 - s} + \tilde{d}_{bf} \qquad (7)$$

represents the transition from the channel b to the final state 'f'. $\hat{G}_f$ corresponds to a tree diagram for the transition from initial channel (γN in the case photoproduction) to the state 'f':

$$\hat{G}_f = \sum_\alpha \frac{g_{\gamma N}^{(\alpha)} g_f^{(\alpha)}}{M_\alpha^2 - s} + \tilde{h}_{(\gamma N)f}\,. \qquad (8)$$

Direct non-resonant transitions to the $\eta' N$ final state $\tilde{d}_{bf}$ and $\tilde{h}_{(\gamma N)f}$ were set to zero in this analysis and only the decay couplings $g_f^{(\alpha)}$ were fitted as free parameters.

The forward peak in the differential cross section at high energies is described by a Reggeized $\rho(\omega)$-meson exchange amplitude [14, 15]. If the $\eta' N$ photoproduction data are fitted with Eqn. (5) the projection of the t,u-channel amplitude into partial waves only contributes to the $\tilde{h}_{(\gamma N)f}$ term. If the $\eta' N$ channel is taken into account as a channel, the t,u-channel amplitudes should contribute also to the P-vectors and to the full amplitude due to rescattering via a $\eta' N$ meson loop diagram. However, such a contribution is very small compare to the other components (e.g. nonresonant transition to πN channel) and can be neglected in the fit.

With $g(t) = g_0 \exp(-bt)$ as vertex function and form factor, $\alpha(t)$ as trajectory, $\nu = \frac{1}{2}(s-u)$, ν_0 as normalization factor, we obtain [14]:

$$A = g(t) \cdot \frac{e^{-i\frac{\pi}{2}\alpha(t)}}{\cos(\frac{\pi}{2}\alpha(t))} \left(\frac{\nu}{\nu_0}\right)^{\alpha(t)}\,. \qquad (9)$$

2

To eliminate the poles at $t < 0$, additional Γ-functions are introduced in (9) by replacing

$$\cos\left(\frac{\pi}{2}\alpha(t)\right) \rightarrow \cos\left(\frac{\pi}{2}\alpha(t)\right)\ \Gamma\left(\frac{\alpha(t)}{2}+\frac{1}{2}\right). \quad (10)$$

The $\rho(\omega)$ trajectory is parametrized as

$$\rho(\omega) \qquad \alpha(t) \;=\; 0.50 + 0.85(\mathrm{GeV}^{-2})t \qquad (11)$$

where t is given in GeV^2. The amplitude A in Eq. (9) is related to the cross section by

$$\frac{d\sigma}{dt} = \frac{1}{64\pi sk^2}|A|^2 \qquad (12)$$

3. Fits to the data on $\gamma p \rightarrow \eta' p$

In addition to the data on η' production, we used further data to constrain the amplitudes. We used the results on the real and imaginary part of the πN scattering amplitude for the partial waves up to $J = 9/2^{\pm}$ from Ref. [20] and data on pion and photoproduction data with πN, ηN, $K\Lambda$, $K\Sigma$, $N\pi^0\pi^0$, and $N\pi^0\eta$ in the final state. A list of the data with references can be found on our web page (pwa.hiskp.uni-bonn.de/). This primary fit was used for a study of $N^* \rightarrow N\omega$ [18], $\rightarrow N\eta$ [21], $\rightarrow K^*\Lambda$ [22], and now for $N\eta'$ decays.

The primary fits for this analysis used all data listed above except those on $\gamma p \rightarrow p\omega$ and $\gamma p \rightarrow K^{*+}\Lambda$. Different primary fits were made, all gave a good description of the data. The fits differed in the number of K-matrix poles assumed to contribute to the $J^P = 3/2^+$ partial wave (corresponding to resonances at 1720, 1900, 2200, with or without a resonance at 1960 MeV), two or three resonances in the $J^P = 5/2^+$ partial wave (at 1680 and 1860 and/or 2100 MeV), different helicity couplings for $N(1990)7/2^+$. Furthermore, resonances above 2 GeV with spin parities up to $J = 7/2$ were added (one by one) in all partial waves. Sometimes a better fit was achieved but the gain in χ^2 was not sufficient to claim evidence for new resonances.

For most fits which included the data on $\gamma p \rightarrow \eta' p$, all parameters of one of these fits were frozen, and only additional $N\eta'$ decay were admitted. These fits used different primary fits and resulted in a variation of $N^* \rightarrow N\eta'$ branching ratios. In final fits, all parameters were varied but they remained stably in the local minimum.

For reaction $\gamma p \rightarrow \eta' p$, the following data were included: The differential cross sections from the CBELSA/TAPS (CBT) experiment [9] cover the range from threshold to 2360 MeV in invariant mass. The data are divided into 20 mass bins and 10 bins in $\cos\theta$, where θ gives the η' direction in the center-of-mass system. The more recent CLAS publication on the process [8] reported differential cross sections up to W=2840 MeV, in 40 mass bins and 20 angular bins with superior statistics. The existence of two different data sets with different systematics allows for valuable cross checks on the results from the two experiments.

The CLAS differential cross sections have a systematic uncertainty of about 12%, which, when used as a scaling factor in the fit, helped increase the compatibility of the CLAS and CBELSA/TAPS differential cross sections. In
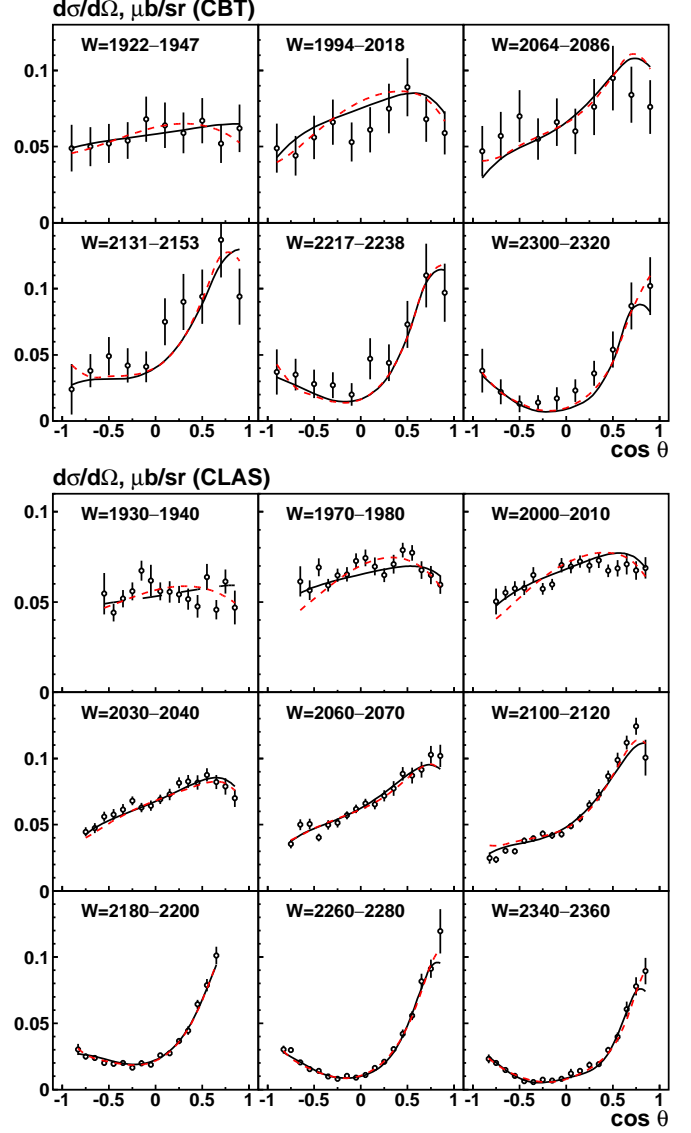

Figure 1: (Color online) Selected data for the $\gamma p \rightarrow \eta' p$ differential cross section from CBELSA/TAPS [9] (top) and from CLAS [8] (bottom). Fit 1 is shown by solid (black) curves and fit 2 by dashed (red) curves. The PWA-curves shown in comparison to the CLAS data are scaled by an energy and angle independent global scaling factor of 0.9.

the fits, the CLAS differential cross sections were multiplied with a scaling factor $1/f$; the fit returned a scaling factor 0.9. Thus, the curves shown for the CLAS differential cross section are multiplied with 0.9. Likewise, the systematic uncertainty of 6% for the beam asymmetry data from CLAS [13] was incorporated, and the predicted beam asymmetry from the fit was found to be larger by 6% than the data. Beyond these three experiments, most existing data on pion- and photo-induced reactions leading to two or three particles in the final state were included in the fit;

Table 1: The description of the dataset for the reaction $\gamma p \to \eta' p$ (χ^2/N_{data}) used in obtaining the two partial-wave solutions discussed in the text. The remainder of the data used in the fits is described in Ref. [23–25].

	N_{data}			χ^2/N_{data} Fit 1	χ^2/N_{data} Fit 2
$d\sigma/d\Omega$	200	CBT	[9]	1.11	1.05
$d\sigma/d\Omega$	524	CLAS	[8]	1.40	1.53
Σ	14	GRAAL	[12]	1.49	1.55
Σ	56	CLAS	[13]	1.78	1.64
total	794	all		1.42	1.46

the dataset is described more fully in Refs. [23–25].

As might be expected when many parameters are involved, the fits of the formalism to this dataset did not converge to a unique minimum with a single set of parameters. In the fits, we studied the impact of different choices of high-mass resonances. The properties of most resonances remained stable. For the reaction $\gamma p \to \eta' p$, two distinct classes of minima were found with a very similar fit quality (expressed as a total χ^2). Table 1 gives the number of data points, the total χ^2/N_{data}, and the breakdown of the individual contributions. Figure 1 shows the differential cross sections from the CBELSA/TAPS and CLAS experiments for selected mass bins, indicating the general quality of the fit obtained. In general, the description of the data is very good. At high masses, the CBELSA/TAPS differential cross section data are not fully compatible with the CLAS data; instead the former results tend to be larger. Nevertheless, both datasets can be fit simultaneously when the relative normalization is allowed to adjust the data within the stated systematic uncertainties. The resulting fit χ^2 values are excellent for both datasets.

Figure 2 shows data for the beam asymmetry Σ from the GRAAL [12] and the CLAS [13] experiment. GRAAL reported Σ for two mass bins just above the threshold. Surprisingly, the photon beam asymmetry is already considerably strong just 7 MeV above the threshold and then weaker at 16 MeV above the threshold. This rapid change in magnitude points to large interferences among multiple resonances below the η' production threshold. The GRAAL beam asymmetry data could not be fit, however, unless solutions were accepted where other data were badly described and/or where some N^* had very large $N^* \to N\eta'$ coupling constants. In the end, we accepted that the GRAAL data at 1903 MeV could not be fully reproduced.

The CLAS data on the beam asymmetry are also shown in Fig. 2. Overall, the fit obtained is reasonable, though the fit trend is smoother than the data. The disagreement between fit and data is slightly larger than the statistical uncertainties for several points, and, as a result, the χ^2 per data point is larger than 1 (see Table 1).

4. Partial-wave content of the fit to $\gamma p \to \eta' p$

Having arrived at two reasonable descriptions of the differential cross section and photon beam asymmetry data, predictions of those fits for the total cross section can be made and the importance of the contributions to the total cross section from various resonances can be assessed. In comparing the CLAS data to the results of the fit, the total cross section for the $\gamma p \to \eta' p$ reaction can be obtained by summation of the differential cross sections over the solid angle, using the PWA fit result for those regions of solid angle not covered by the CLAS results.

The resulting total cross section predictions from the two fits described above are shown in Fig. 3. Also shown in the figure are the most important partial-wave contributions to the total cross section from both fits. As seen in the figure, at and slightly above the threshold, the $N(1895)1/2^-$ resonance is seen to dominate the reaction in both solutions. This resonance matches the characteristic energy, spin, and parity suggested in the previous analyses of the differential cross section data mentioned in the Introduction, where all agreed that the threshold region was governed by a resonance with $J^P = 1/2^-$ and a mass of about 1900 MeV. The $N(1895)1/2^-$ state is a "two star" resonance in the most recent Review of Particle Physics (RPP) [28]. Also common to both our solutions is the strong contribution of the $N(1900)3/2^+$ excited state, a "three-star" resonance in the RPP. With respect to the fits reported here, however, the contributions from $N(2100)$ $1/2^+$ and $N(2120)3/2^-$ were found to be significantly different in the two fits arrived at here. Small contributions were seen in the fits from the $N(2060)5/2^-$ and $N(2000)5/2^+$ resonances, but those are not shown in Fig. 3.

To investigate improvements of the fit with additional resonances in the mass region above 2200 MeV, additional poles were added to the K-matrix, one-by-one, with the resulting χ^2 computed. The additional poles had spin-parities of $J^P = 1/2^\pm$, $3/2^\pm$, $5/2^\pm$, $7/2^\pm$. Although each additional state improved the quality of the fit somewhat based on χ^2, no fit with an additional contribution was obviously superior to another. Instead, the variations in the parameters resulting from these additions were used to estimate the model dependence of the results for the fits.

In Table 2, the branching ratios deduced from these fits for $N^* \to N\eta'$ decays are presented for the six resonances used in both fits. Two of these resonances have masses very close to the η' production threshold. Branching ratios are usually defined at the nominal mass of a resonance and vanish identically when the threshold is above the nominal mass. However, due to the finite width of nucleon excitations (typically 100 MeV or more), a resonance with a mass below the η' threshold may nevertheless still decay into a final state that lies above the η' threshold.
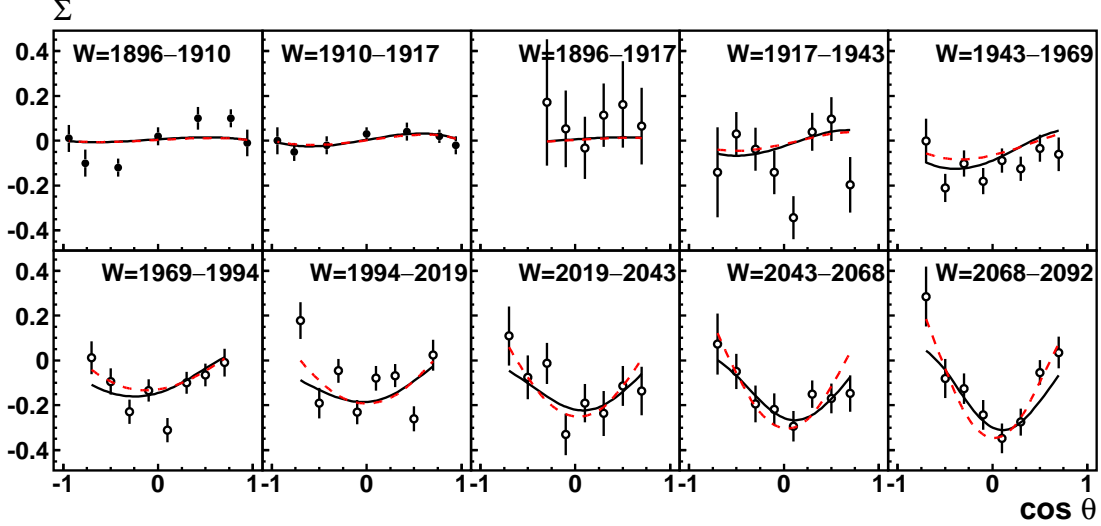
Figure 2: (Color online) The beam asymmetry Σ for the reaction $\gamma p \to \eta' p$. Shown are data from GRAAL [12] (first two subfigures) and recent data from CLAS [13] (next eight subfigures). Also shown are the results of each of the two partial-wave solutions discussed in the text. Fit 1 is shown by solid (black) curves and Fit 2 with dashed (red) curves. The PWA-curves for the CLAS beam asymmetries are scaled by a factor 0.94.

Table 2: Branching ratios (in %) for N^* resonance decays into $N\eta'$ final states based on the two partial-wave fits discussed in the text.

	Fit 1		Fit 2	
Resonance	B.R.	$\delta(\chi^2)$	B.R.	$\delta(\chi^2)$
$N(1895)1/2^-$	11±3	74	14±5	90
$N(2100)1/2^+$	8±2	105	7±2	150
$N(2120)3/2^-$	3±1	123	4±2	242
$N(1900)3/2^+$	6±2	137	6±2	101
$N(2060)5/2^-$	<1	3	<1	6
$N(2000)5/2^+$	<1	2	2±1	11

Therefore, we use a different definition:

$$BR = \int\limits_{\text{threshold}}^{\infty} \frac{ds}{\pi} \frac{f(g_a^\alpha)^2 \rho_a^\alpha(s)}{(M_{\text{BW}}^\alpha{}^2 - s)^2 + f^2(\sum_\alpha g_a^\alpha{}^2 \rho_a^\alpha(s))^2} \quad (13)$$

The Breit-Wigner mass and the parameter f are adjusted so that its pole matches the pole position of the full amplitude, f is typically in the range $0.9-1.1$. The uncertainties in the branching ratios cover the variations seen in these branching ratios when different primary fits were used.

Also given in Table 2 are the changes in χ^2_{tot} when one of the resonances is omitted from the fit. The uncertainties in the branching ratios were estimated from the spread of results obtained by adding one of the high-mass resonances. In most cases, the uncertainties have sizes which are similar to the differences between Fit 1 and Fit 2. We therefore combined these differences with the uncertainties in Table 2 and find the final results which are collected in Table 3.

In Table 3 we also present pole positions, helicity couplings, and other branching ratios which are taken from

[18, 25, 27]. The branching ratios for decays into $K\Lambda$ and $K\Sigma$ will be presented in a forthcoming publication. In two cases, the sum of the observed branching ratios exceeds 1 but is still compatible with 1 when the large errors are considered.

The uncertainties in the branching ratios in Table 3 are ranges within which a fit solution is possible. While these uncertainties are relatively large, the four resonances do have statistically significant branches to $N\eta'$ based on the analysis reported here. The statistical evidence for the η' decay mode should be judged from the change in χ^2 when a resonance is removed (see Table 2) and not from the total uncertainties in Table 3.

The most recent RPP does not report any observed branching ratios for decays into $N\eta'$. This analysis suggests that statistically significant $N\eta'$ branches exist for four of the six states indicated in Table 2. If confirmed, these branches represents a useful test for any model for the decays of those states based on, for example, a quark description of the nucleon, especially when combined with similar data for η photoproduction on the nucleon.

The ambiguities in the parameters and resonances observed in the partial-wave analyses conducted here might be resolved by further data on η' photoproduction, as well as additional data on spin observables for the photoproduction of other mesons from the nucleon. With respect to η', the CBELSA/ TAPS collaboration has presented preliminary results on the helicity difference $E = (\sigma_{1/2} - \sigma_{3/2})/(\sigma_{1/2} + \sigma_{3/2})$ for the $\gamma p \to \eta' p$ reaction [29]. Since those data are preliminary, those data were not yet included in the present fits. However, when finalized, those results may help to discriminate between the two fit solutions and to better constrain the parameters and branching ratios obtained in this work. With that in mind, Figure 4

Table 3: Results on the four resonances with significant $N\eta'$ decay branchings ratios. The masses and widths $M_{\rm pole}$,$\Gamma_{\rm pole}$ are given in MeV, the moduli of the helicity couplings in $10^{-3}\,{\rm GeV}^{-1/2}$. Other branching ratios are given for comparison. $\Delta\pi$ denotes $\Delta(1232)3/2^+\pi$ and $N^*\pi$, $N(1520)3/2^-\pi$.

| | $M_{\rm pole}$ | $\Gamma_{\rm pole}$ | $A_{1/2}$ phase | $A_{3/2}$ phase | Branching ratios (in %) for $N^* \to$ |
					$N\eta'$	$N\pi$	$N\eta$	$N\omega$	$\Delta\pi$	$N^*\pi$	$N\sigma$
$N(1895)1/2^-$	1907 ± 10	100^{+40}_{-10}	-15 ± 6 $-(35\pm35)$		13 ± 5	2.5 ± 1.5	10 ± 5	28 ± 12	7 ± 4	-	-
$N(2100)1/2^+$	2100 ± 30	280 ± 35	-6 ± 4 (10 ± 25)	12 ± 5 (70 ± 30)	8 ± 3	16 ± 5	25 ± 10	15 ± 10	10 ± 4	30 ± 4	20 ± 6
$N(2120)3/2^-$	2115 ± 40	345 ± 35	130 ± 45 $-(40\pm25)$	160 ± 60 $-(30\pm15)$	4 ± 2	5 ± 3	3 ± 2	12 ± 8	70 ± 23		11 ± 4
$N(1900)3/2^+$	1910 ± 30	280 ± 50	26 ± 14 (60 ± 35)	-70 ± 30 (70 ± 50)	6 ± 2	3 ± 2	3 ± 1	15 ± 9	50 ± 15	15 ± 8	4 ± 3

shows our prediction for the helicity asymmetry E for the $\gamma p \to \eta'p$ reaction based on the two partial-wave solutions found in this work.

5. Conclusion

We have included new data on the reaction $\gamma p \to \eta'p$ in a fit to the BnGa database for meson photoproduction. A partial-wave analysis identifies the leading resonance contributions and provides additional support for the existence of $N(1895)1/2^-$, $N(1900)3/2^+$, $N(2100)1/2^+$, and $N(2120)3/2^-$. When analyzed in terms of these resonances, statistically significant branching ratios for their decays into $N\eta'$ were determined. In the most recent PDG summary, no such branches are indicated as having been seen. Additional data on spin observables should help pin down the issue of whether these branches to $N\eta'$ are present for the resonances of Table 2, which, in turn, will help test models of the nucleon.

6. Acknowledgments

References

[1] [Aachen-Berlin-Bonn-Hamburg-Heidelberg-Munich Collaboration], Phys. Rev. **175**, 1669 (1968).

[2] W. Struczinski *et al.* [Aachen-Hamburg-Heidelberg-Munich Collaboration], Nucl. Phys. B **108**, 45 (1976).

[3] R. Plötzke *et al.* [SAPHIR Collaboration], Phys. Lett. B **444**, 555 (1998).

[4] W. T. Chiang, S. N. Yang, L. Tiator, M. Vanderhaeghen and D. Drechsel, Phys. Rev. C **68**, 045202 (2003).

[5] M. Dugger *et al.* [CLAS Collaboration], Phys. Rev. Lett. **96**, 062001 (2006) Erratum: [Phys. Rev. Lett. **96**, 169905 (2006)].

[6] L. Tiator, Int. J. Mod. Phys. A **22**, 297 (2007).

[7] F. Huang, H. Haberzettl and K. Nakayama, Phys. Rev. C **87**, 054004 (2013).

[8] M. Williams *et al.* [CLAS Collaboration], Phys. Rev. C **80**, 045213 (2009).

[9] V. Crede *et al.* [CBELSA/TAPS Collaboration], Phys. Rev. C **80**, 055202 (2009).

[10] I. Jaegle *et al.* [CBELSA/TAPS Collaboration], Eur. Phys. J. A **47**, 11 (2011).

[11] V. L. Kashevarov *et al.*, Phys. Rev. Lett. **118**, no. 21, 212001 (2017).

[12] P. Levi Sandri *et al.*, Eur. Phys. J. A **51**, no. 7, 77 (2015).

[13] P. Collins *et al.*, "Photon beam asymmetry Σ for η and η' photoproduction from the proton," arXiv:1703.00433 [nucl-ex].

[14] A. Anisovich, E. Klempt, A. Sarantsev and U. Thoma, Eur. Phys. J. A **24**, 111 (2005).

[15] A. V. Sarantsev, A. V. Anisovich, V. A. Nikonov and H. Schmieden, Eur. Phys. J. A **39**, 61 (2009).

[16] A. V. Anisovich and A. V. Sarantsev, Eur. Phys. J. A **30**, 427 (2006).

[17] A. V. Anisovich, V. V. Anisovich, E. Klempt, V. A. Nikonov and A. V. Sarantsev, Eur. Phys. J. A **34**, 129 (2007).

[18] I. Denisenko *et al.*, Phys. Lett. B **755**, 97 (2016).

[19] S. U. Chung, J. Brose, R. Hackmann, E. Klempt, S. Spanier and C. Strassburger, Annalen Phys. **4**, 404 (1995).

[20] R. A. Arndt, W. J. Briscoe, I. I. Strakovsky and R. L. Workman, Phys. Rev. C **74**, 045205 (2006).

[21] J. Müller *et al.* [CBELSA/TAPS Collaboration], submitted to Phys. Lett. (2017).

[22] A. V. Anisovich *et al.* [CBELSA/TAPS Collaboration], submitted to Phys. Lett. (2017).

[23] A. V. Anisovich, R. Beck, E. Klempt, V. A. Nikonov, A. V. Sarantsev and U. Thoma, Eur. Phys. J. A **48**, 15 (2012).

[24] E. Gutz *et al.* [CBELSA/TAPS Collaboration], Eur. Phys. J. A **50**, 74 (2014).

[25] V. Sokhoyan *et al.* [CBELSA/TAPS Collaboration], Eur. Phys. J. A **51**, no. 8, 95 (2015) Erratum: [Eur. Phys. J. A **51**, no. 12, 187 (2015)].

[26] T. Sekihara, S. Sakai and D. Jido, Phys. Rev. C **94**, no. 2, 025203 (2016).

[27] J. Müller et al. [CBELSA/TAPS Collaboration], *New data on with polarized photons and protons and their implications for* $N^* \to N\eta$ *decays*, submitted to Physics Letters B.

[28] C. Patrignani *et al.* [Particle Data Group], Chin. Phys. C **40**, no. 10, 100001 (2016).

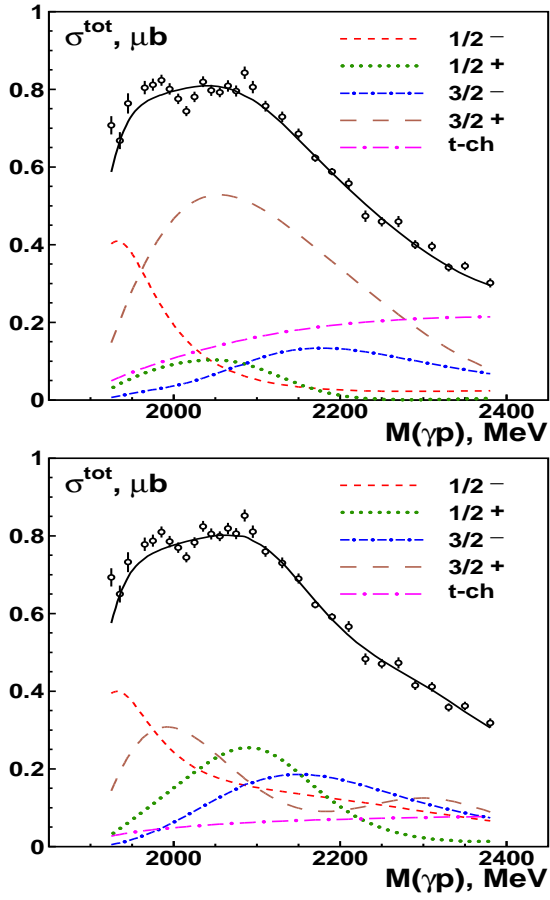[29] F. N. Afzal [CBELSA/TAPS Collaboration], EPJ Web Conf. **37**, 09001 (2012).

Figure 3: (Color online) The total cross section for $\gamma p \to \eta' p$ and the partial wave contributions with defined spin-parity J^P from the two partial-wave solutions described in the text. Data shown are extrapolated, as discussed in the text, from the CLAS data of Ref. [8]. The long-dashed - dotted curve represents the contribution from t-channel exchanges. The $1/2^\pm$ and $3/2^\pm$ partial waves in the figure contain the contribution from t-channel exchange in the particular partial wave.
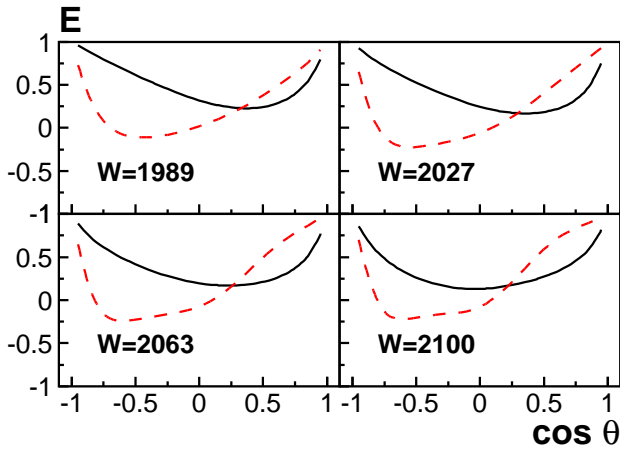

Figure 4: (Color online) Prediction of the helicity asymmetry E for Fit 1, solid (black) curve and for Fit 2, dashed (red) curve.